The TRPC5 channel regulates angiogenesis and promotes recovery from ischemic injury in mice

Received for publication, August 15, 2018, and in revised form, November 6, 2018 Published, Papers in Press, November 9, 2018, DOI 10.1074/jbc.RA118.005392

Yifei Zhu[‡§1], Mengru Gao[‡1], Tingting Zhou[‡1], Mingxu Xie[‡§], Aiqin Mao[‡], Lei Feng[‡], Xiaoqiang Yao[§], Wing Tak Wong[¶], and Xin Ma[‡2]

From the [‡]Wuxi School of Medicine, Jiangnan University, Wuxi, Jiangsu 214000, China and the [§]School of Biomedical Sciences and [¶]State Key Laboratory of Agrobiotechnology (CUHK), School of Life Sciences, Chinese University of Hong Kong, Hong Kong 999077, China

Edited by Xiao-Fan Wang

Ischemia-related diseases are a leading cause of death worldwide, and promoting therapeutic angiogenesis is key for effective recovery from hypoxia–ischemia. Given the limited success of angiogenic factors, such as vascular endothelial growth factor, in clinical trials, it is important to find more promising angiogenic targets. Here, using both cell- and tissue-based assays and a mouse model of injury-induced ischemia, we investigated the involvement of the transient receptor potential canonical 5 (TRPC5) ion channel in angiogenesis and the effects of a TRPC5 activator, the Food and Drug Administration–approved drug riluzole, on recovery from ischemic injury. We demonstrate that TRPC5 is involved in endothelial cell sprouting, angiogenesis, and blood perfusion in an oxygen-induced retinopathy model and a hind limb ischemia model. We found a potential regulatory link between nuclear factor of activated T cell isoform c3 and angiopoietin-1 that could provide the mechanistic basis for the angiogenic function of TRPC5. Importantly, treatment with riluzole, which can activate TRPC5 in endothelial cells, improved recovery from ischemia in mice. Our study reveals TRPC5 as a potential angiogenic target and suggests riluzole as a promising drug for managing ischemic diseases.

Ischemia resulting in occlusion of blood supply and tissue hypoxia can lead to various vascular diseases. Conditions associated with tissue ischemia, such as coronary heart disease, myocardial infarction, carotid artery disease, peripheral arterial disease and ischemic stroke, are leading causes of death worldwide, with high prevalence in aging populations and high sociodemographic regions (1, 2). Current drug therapies for ischemia-related diseases include the antiplatelet/antithrombotic drug aspirin, cholesterol-modifying statins, and blood pressure reducers such as angiotensin-converting enzyme inhibitors, angiotensin receptor blockers, and β blockers (3). However, these commonly used therapies are usually unable to restore sufficient blood flow in a timely manner to fully eliminate symptoms and develop drug resistance (4–6). Although traditional surgical bypass treatment along with medical therapy show better efficacy than medical therapy alone, and endovascular intervention is associated with decreased periprocedural morbidity and mortality, the therapeutic effects are still limited, including high risk of restenosis, unknown durability, and so on (7–9). Therapeutic angiogenesis to promote blood flow is therefore key when treating ischemia-related diseases (4, 5, 10).

Angiogenesis is a multistep process involving sprouting, proliferation, migration, tube formation, branching, and anastomosis of endothelial cells (ECs)[3] that is highly regulated by three main pathways: Notch/Dll4, which regulates EC sprouting; the VEGF signaling pathway, which initiates angiogenesis; and the Angiopoietin-1/Tie2 pathway, which regulates vascular maturation and vessel remodeling (11). Clinical trials of angiogenic therapy for ischemic diseases have involved cell-based therapy and gene therapy to deliver pro-angiogenic factors such as VEGF and fibroblast growth factor to the damaged areas (12). However, cell therapy involved a lot of work to ensure safety and patient benefits, and to date, none of the investigated pro-angiogenic factors have been shown to have clinical utility (13–17). Therefore, it is crucial to identify other key angiogenic factors with potential for treating ischemia-related diseases.

Intracellular Ca^{2+} ($[Ca^{2+}]_i$), particularly that driven by Ca^{2+} influx, in ECs is a key regulator of angiogenesis (18). It has been reported that ECs decode VEGF-mediated Ca^{2+} signaling to exercise different functions (19). Orais, Piezo, and transient receptor potential (TRP) channels are expressed in ECs and modulate $[Ca^{2+}]_i$, which regulates several physiological processes, including angiogenesis (18, 20–22). The canonical TRP family members TRPC1, TRPC3, TRPC4, and TRPC6 have all been reported to be involved in cell migration, proliferation, tube formation, and angiogenesis (23–26). However, under

This work was supported by the National Natural Science Foundation of China Grants 81572940, 81622007, 81800430, and 81870362, Chang Jiang Scholars Programme (Q2015106), Fundamental Research Funds for the Central Universities Grants JUSRP51704A and JUSRP51615B, and National First-Class Discipline Program of Food Science and Technology Grant JUFSTR20180101. The authors declare that they have no conflicts of interest with the contents of this article.

This article contains Figs. S1–S5 and Table S1.

[1] These authors contribute equally to this work.

[2] To whom correspondence should be addressed: Wuxi School of Medicine, Jiangnan University, 1800 Lihu Rd., Wuxi, China. Tel.: 86-510-85914599. E-mail: maxin@jiangnan.edu.cn.

[3] The abbreviations used are: EC, endothelial cell; VEGF, vascular endothelial growth factor; TRP, transient receptor potential; MMEC, mesenteric vascular endothelial cell; OIR, oxygen-induced retinopathy; PD, postnatal day; NVT, neovascular tuft; HLI, hind limb ischemia; AAV, adeno-associated virus; HMEC, human microvascular endothelial cell; FDA, Food and Drug Administration; EGM, endothelial cell growth medium; ANOVA, analysis of variance.

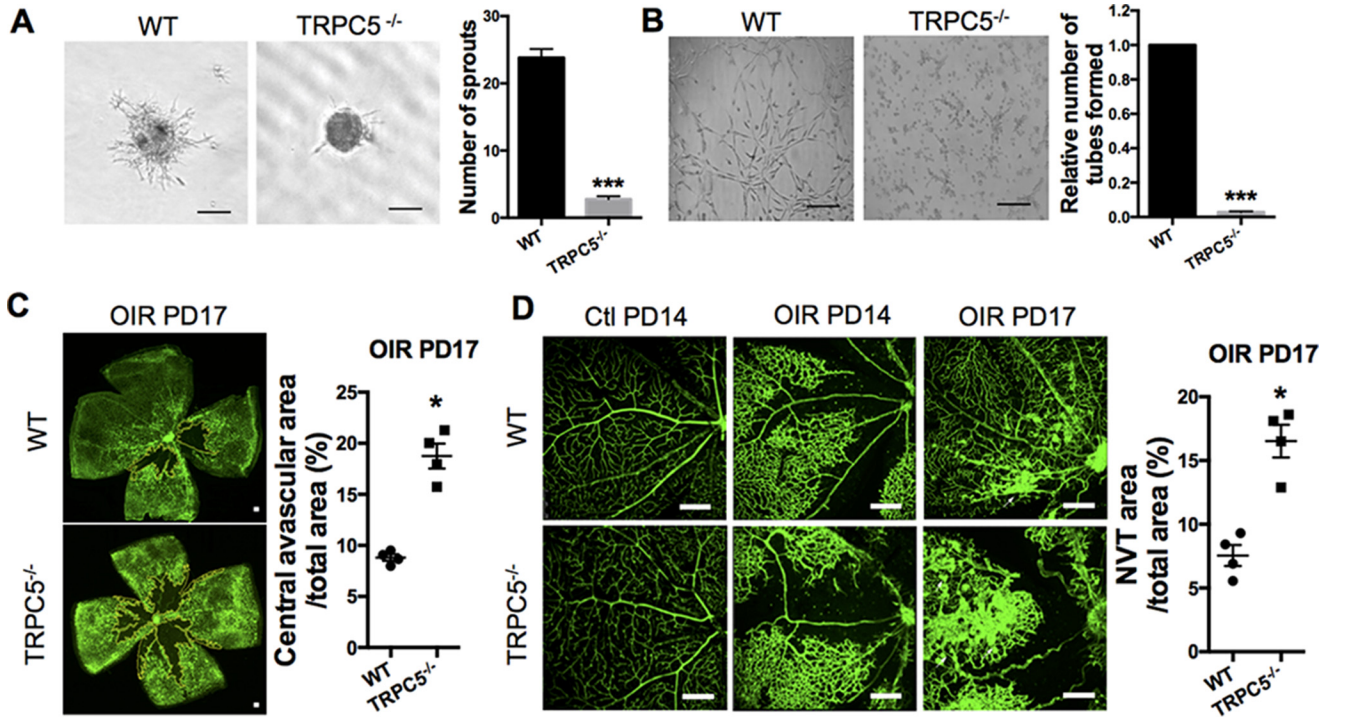

Figure 1. TRPC5 is involved in hypoxia-induced EC sprouting and mouse retinal angiogenesis. *A*, under 1% O_2 hypoxia, primary MMECs from WT or TRPC5$^{-/-}$ mice were allowed to form spheroids for 24 h, followed by collagen embedding for another 24 h to form sprouts. *Left panel*, representative images showing the sprouting spheroids of MMECs from WT and TRPC5$^{-/-}$ mice under hypoxia. *Right panel*, morphometric analysis of sprout numbers per spheroid. $n = 8$ independent experiments. ***, $p < 0.001$ *versus* WT, unpaired *t* test with Welch's correction. *B*, *left panel*, representative images of tube formation of WT and TRPC5$^{-/-}$ MMECs that were seeded on Matrigel under hypoxic conditions for 10 to 14 h. *Right panel*, tube formation was quantitated as the number of tube-like structures in five randomly selected microscopic fields. $n = 6$ independent experiments. ***, $p < 0.001$ *versus* WT, Wilcoxon signed-rank test. *C*, pathological neovascularization upon OIR in WT and TRPC5$^{-/-}$ mice. Neonatal mice exposed to 75% O_2 hyperoxia from PD7 to PD12 and 21% O_2 normoxia from PD12 to PD17. *Left panel*, representative images of the isolectin B4-Alexa 488-positive (*green*) blood vessels of retinas with vaso-obliteration regions (outlined in *yellow*) at PD17. *Right panel*, quantification of the central avascular areas of retinas from WT and TRPC5$^{-/-}$ mice at PD17 in the OIR model. $n = 4$ independent experiments. *, $p < 0.05$ *versus* WT, unpaired Mann–Whitney test. *D*, representative images showing the retinal vasculature of control (PD14) and OIR (PD14 and PD17) mice. Vaso-obliteration was found in PD14 OIR retinas but not in control PD14 retinas. The *white arrows* indicate NVTs in PD17 OIR retinas. A statistical analysis of the NVT area in PD17 OIR retinas is shown on the *right*. $n = 4$ independent experiments. *, $p < 0.05$ *versus* WT, unpaired Mann–Whitney test. *A–D*, the values are means ± S.E. *Scale bars* = 100 μm (*A* and *B*), 500 μm (*C*), and 250 μm (*D*).

hypoxia–ischemia conditions, the involvement of the TRPC channel in angiogenesis is unknown. Therefore, we decided to examine whether the TRPC channel is involved in angiogenesis under conditions of hypoxia and whether it presents a suitable therapeutic option for ischemic tissue recovery. Using two mouse models of ischemia and ECs from TRPC5 knockout mice, we found that TRPC5 is involved in angiogenesis and that application of riluzole, an approved clinical drug and activator of TRPC5, can improve ischemia recovery in mice.

Results

TRPC5 plays a role in EC sprouting under hypoxia and ischemic mouse retinal angiogenesis

To examine the involvement of TRPC proteins in angiogenesis, we first evaluated their role in EC sprouting, a key step in angiogenesis (11). Using primary mouse intestinal mesenteric vascular endothelial cells (MMECs), we examined cell sprouting under hypoxia by spheroid capillary sprouting assays. The number of sprouts was decreased upon siRNA-mediated knockdown of TRPC1, TRPC3, TRPC4, TRPC5, and TRPC6 (Figs. S1 and S2). Because the least number of sprouts was found upon knockdown of TRPC5, and less research has been done to look for the relationship between TRPC5 and angiogenesis, we decided to confirm the involvement of TRPC5 using primary MMECs from WT and TRPC5 knockout (TRPC5$^{-/-}$) mice by spheroid capillary sprouting and tube formation assays (Fig. 1, *A* and *B*). Under hypoxia, both EC sprouting and tube formation were significantly inhibited in MMECs from TRPC5$^{-/-}$ mice, suggesting a role for TRPC5 in angiogenesis.

To validate these *in vitro* observations, we investigated the angiogenic role of TRPC5 in mice using oxygen-induced retinopathy (OIR) as a model of ischemia-induced retinal neovascularization. Using TRPC5$^{-/-}$ mice, the effects of TRPC5 deletion on the vascular alterations characteristic of OIR were investigated in a relative hypoxia model (27). WT and TRPC5$^{-/-}$ neonatal mice were exposed to 75% oxygen at postnatal day (PD) 7 for 5 days and then returned to 21% oxygen (room air) for another 5 days (PD12 to PD17). Hyperoxia induces rapid central vaso-obliteration, which becomes hypoxia when mice return to room air (28). In OIR, the superficial vascular plexus has been observed to be characterized by a pronounced avascular area without morphologic signs of neovascularization at PD12, followed by neovascular tuft (NVT) formation, which is pathological neovascularization, that begins to emerge at PD15 between the central avascular area and the peripheral vascularized retina (27, 29). Consistent with prior observations of pathological neovascularization (27), both WT and TRPC5$^{-/-}$ mouse retinas exhibited avascular areas

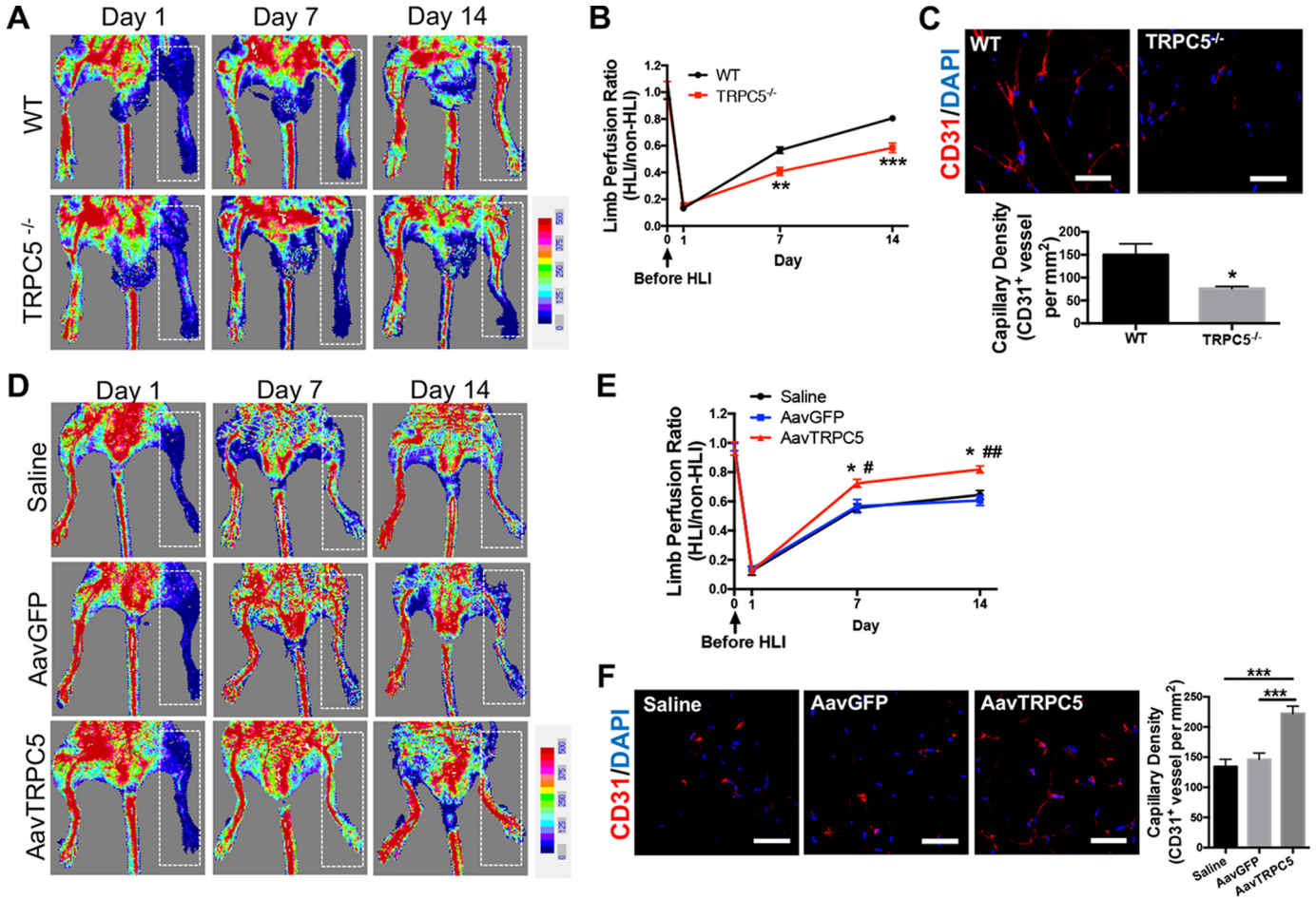

Figure 2. TRPC5 contributes to recovery from hind limb ischemia injury by promoting angiogenesis. *A*, HLI was surgically induced in WT and TRPC5$^{-/-}$ mice. Blood flow was determined by laser Doppler imaging on days 1, 7, and 14 after HLI. Ischemic limbs are highlighted by *white dashed boxes*. *B*, comparison of limb perfusion ratios between WT and TRPC5$^{-/-}$ mice measured on days 1, 7, and 14 after HLI. The final blood flow values are expressed as the ratios of ischemic to nonischemic hind limb perfusion. $n = 7$ to 8. Day 7: **, $p < 0.01$ *versus* WT; Student's unpaired two-tailed *t* test. Day 14: ***, $p < 0.001$ *versus* WT; unpaired Mann–Whitney test. *C*, immunofluorescent staining for CD31 (*left*) and quantitation of blood vessel densities (*right*) in adductor muscle sections from the injured limbs of WT and TRPC5$^{-/-}$ mice on day 14 after HLI. For the capillary and arteriole density assessments, the numbers of capillaries and arterioles were counted in five high-powered fields in each of the four tissue sections (per mouse) and then expressed as CD31^{+} vessels per square millimeter. $n = 7$ to 8. *, $p < 0.05$ *versus* WT, unpaired *t* test with Welch's correction. *Scale bars* = 50 μm. *D*, C57BL/6J mice were injected with an adeno-associated virus coding for TRPC5 (*AavTRPC5*) or GFP (*AavGFP*) or with saline 7 days before HLI surgery. Ischemic limbs are highlighted by *white dashed boxes*. *E*, limb perfusion ratios of the saline, AavGFP, and AavTRPC5 groups on days 1, 7, and 14 after HLI. The final blood flow values are presented as the ratios of ischemic to nonischemic hind limb perfusion. $n = 6$ to 7. Day 7: *, $p < 0.05$ *versus* saline; #, $p < 0.05$ *versus* AavGFP. Day 14: *, $p < 0.05$ *versus* saline; ##, $p < 0.01$ *versus* AavGFP. Dunn's multiple comparisons test. *F*, immunofluorescent staining for CD31 (*left panel*) and quantitation of blood vessel densities (*right panel*) in adductor muscle sections from the injured limbs of saline-, AavGFP-, and AavTRPC5-treated mice on day 14 after HLI. $n = 6$ to 7. ***, $p < 0.001$; one-way ANOVA and Dunnett's multiple comparisons test. *Scale bars* = 50 μm. *A–F*, representative laser Doppler images and micrographs. The values are means ± S.E.

and intravitreal vascular areas without morphologic signs of neovascularization at PD12, followed by NVT formation at PD17 (Fig. 1, *C* and *D*). In contrast to WT mouse retinas, TRPC5$^{-/-}$ mouse retinas displayed increased avascular (Fig. 1*C*) and NVT (Fig. 1*D*) areas at PD17, indicating that TRPC5 deletion affects vascular recovery in the OIR model, which, in turn, suggests that endogenous TRPC5 plays a role in preventing vasculopathy exacerbation in ischemic retinas.

TRPC5 contributes to ischemic tissue recovery and angiogenesis in a model of hind limb ischemia

To substantiate a role for TRPC5 in ischemic vascularization, we used a mouse model of hind limb ischemia (HLI). Surgical ischemia was induced in WT and TRPC5$^{-/-}$ mice to assess whether TRPC5 could promote vascular growth and blood flow under ischemic conditions. Laser Doppler imaging showed that although WT mice exhibited nearly complete restoration of blood flow (~80%) 14 days post-HLI, TRPC5$^{-/-}$ mice could only attain ~50% of pre-HLI perfusion ratios (Fig. 2, *A* and *B*). Using an anti-CD31 antibody to identify ECs, we observed that the capillary density in the adductor muscles of injured limbs was significantly lower in TRPC5$^{-/-}$ mice compared with WT mice (Fig. 2*C*).

We next investigated whether overexpression of TRPC5 could promote blood flow restoration and promote ischemic tissue recovery in the HLI model. To this end, an adeno-associated virus (AAV) vector expressing TRPC5 was injected into the hind limbs of C57BL/6J mice 7 days prior to surgical ischemia. Saline or an AAV carrying GFP was used as a control. Higher restoration of blood flow (~80% of limb perfusion ratio) was observed after AAV-TRPC5 delivery on day 14 after HLI, whereas mice in the GFP and saline groups only had ~60% of

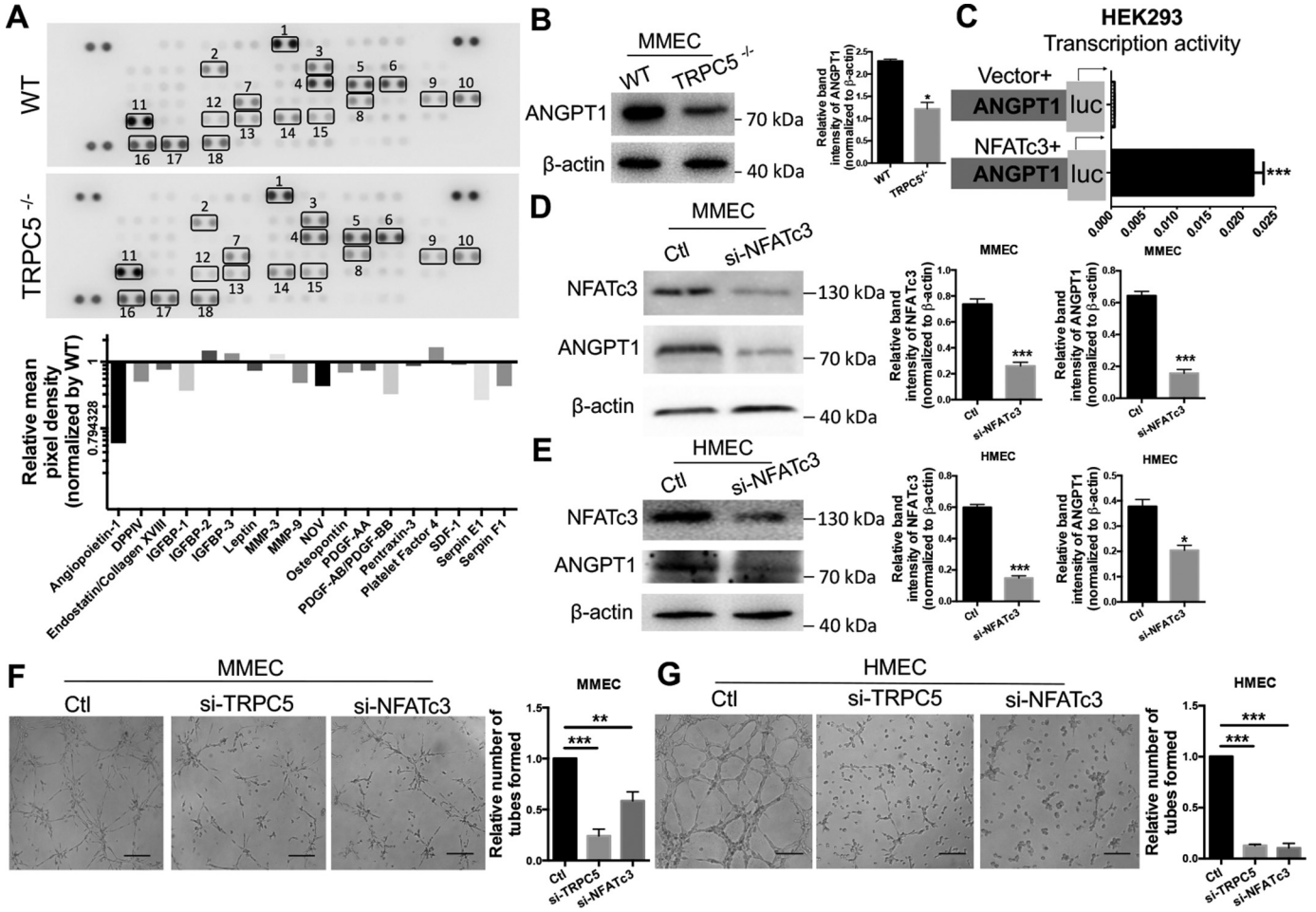

Figure 3. Analysis of interplay between TRPC5, NFATc3, and ANGPT1 in ECs. *A*, *top panel*, detection of differentially regulated angiogenic proteins with an angiogenesis antibody array in WT and TRPC5$^{-/-}$ mouse serum samples. Duplicate spots: *1*, Angiopoietin-1; *2*, DPPIV; *3*, Endostatin/Collagen XVIII; *4*, IGFBP-1; *5*, IGFBP-2; *6*, IGFBP-3; *7*, Leptin; *8*, MMP-3; *9*, MMP-9; *10*, NOV; *11*, Osteopontin; *12*, PDGF-AA; *13*, PDGF-AB/PDGF-BB; *14*, Pentraxin-3; *15*, Platelet Factor 4; *16*, SDF-1; *17*, Serpin E1; *18*, Serpin F1. *Bottom panel*, quantitation of relative protein expression by comparing the mean pixel density of each factor in the TRPC5$^{-/-}$ group with that of each factor in the WT group. *B*, *top*, Western blotting of angiopoietin-1 (ANGPT1) in WT and TRPC5$^{-/-}$ primary MMECs with β-actin as a loading control. The image is representative of three independent experiments. *Bottom*, quantitation of ANGPT1 band intensity relative to β-actin. Values represent means ± S.E. of band intensities from three independent experiments. *, $p < 0.05$ *versus* WT, unpaired Mann–Whitney test. *C*, NFATc3 stimulates the transcriptional activity of ANGPT1 in HEK293 cells co-transfected with NFATc3 and a luciferase reporter plasmid carrying the 5′ flanking the 2012-bp sequence of ANGPT*1*. An empty vector was transfected as a control. The *horizontal axis* indicates relative luciferase activity. $n = 5$. ***, $p < 0.001$ *versus* vector, unpaired *t* test with Welch's correction. *D* and *E*, Western blots (*left panels*) and quantitation (*right panels*) of NFATc3 ($n = 6$) and ANGPT1 ($n = 3$) expression in primary MMECs (*D*) and HMECs (*E*) transfected with NFATc3 siRNA or scrambled siRNA. The band intensities were normalized to β-actin and quantified using ImageJ. ***, $p < 0.001$ *versus* control (*Ctl*), Student's unpaired two-tailed *t* test. *, $p < 0.05$ *versus* Ctl, unpaired Mann–Whitney test. *F* and *G*, representative images of the tube formation in primary MMECs (*F*) and HMECs (*G*) treated with TRPC5 siRNA, NFATc3 siRNA, or control scrambled siRNA. The data are means ± S.E. $n = 5$ to 8. *F*, **, $p < 0.01$; ***, $p < 0.001$ *versus* Ctl; Kruskal–Wallis test and Dunn's multiple comparisons test. *G*, ***, $p < 0.001$ *versus* Ctl, one-way ANOVA and Dunnett's multiple comparisons test. *Scale bars* = 50 μm. *A–E*, representative images are shown, and the values are means ± S.E.

pre-HLI limb perfusion ratios (Fig. 2, *D* and *E*). Immunofluorescence analysis of the ischemic muscles revealed significantly higher blood vessel densities in the AAV-TRPC5 group than in the AAV-GFP or saline control groups (Fig. 2*F*). These data reveal that TRPC5 promotes angiogenesis in an HLI model and might be a promising target for treating ischemia-related diseases.

Involvement of the NFATc3 and ANGPT1 pathway in TRPC5-regulated angiogenesis

To characterize the underlying mechanism of TRPC5-mediated angiogenic effects, we evaluated several angiogenesis-related factors in serum samples from TRPC5$^{-/-}$ and WT mice using an angiogenesis array kit. Among the various factors, angiopoietin-1 (ANGPT1) was markedly down-regulated in TRPC5$^{-/-}$ mouse serum (Fig. 3*A*). We confirmed down-regulation of ANGPT1 protein expression in primary MMECs from TRPC5$^{-/-}$ mice (Fig. 3*B*). Interestingly, ANGPT1 has been reported to contribute to vascular recovery in ischemia (27). Its reported role as a potent pro-angiogenic factor that induces EC migration, tube formation, and sprouting *in vitro* (30) is similar to our findings of TRPC5 roles in the OIR model (Fig. 1), which suggests a relationship between TRPC5 and ANGPT1 in the regulation of angiogenesis.

Because nuclear factor of activated T cell isoform c3 (NFATc3) has been identified previously as a downstream Ca^{2+}-dependent transcription factor of TRPC5 that is translocated to the nucleus upon TRPC5-mediated $[Ca^{2+}]_i$ increases (31), we decided to investigate whether there was any interplay between TRPC5, ANGPT1, and NFATc3. To this end, we eval-

uated whether inhibition or activation of TRPC5 affected ANGPT1 and NFATc3 expression. We found that siRNA-mediated knockdown of TRPC5 in primary MMECs resulted in decreased expression of ANGPT1 and nuclear NFATc3 (Fig. S3*A*). By contrast, treatment of MMECs with riluzole to activate TRPC5 (32, 33) resulted in translocation of NFATc3 from the cytosol to the nucleus and increased expression of ANGPT1 (Fig. S3*B*). Next, we performed additional experiments to determine whether NFATc3 expression correlated with ANGPT1 activity. Luciferase assays revealed that ANGPT1 transcriptional activity was strongly enhanced upon transfection with an NFATc3 plasmid (Fig. 3*C*). Moreover, knocking down NFATc3 by siRNA in primary MMECs (Fig. 3*D*) and human microvascular endothelial cells (HMECs) (Fig. 3*E*) resulted in decreased ANGPT1 expression. Additionally, knocking down NFATc3 by siRNA attenuated tube formation in MMECs (Fig. 3*F*) and HMECs (Fig. 3*G*) with similar efficiency, as seen with siRNA-mediated knockdown of TRPC5. These results suggest the presence of a TRPC5–NFATc3–ANGPT1 signaling axis in angiogenesis.

TRPC5 activation using the approved drug riluzole promotes tissue recovery from ischemia

Because we had found that TRPC5 promotes angiogenesis under ischemic conditions, we decided to evaluate whether the TRPC5 activator riluzole, a Food and Drug Administration (FDA)–approved drug for ALS, can be repurposed for treating ischemia (32, 34). The effect of riluzole on TRPC5 was verified by Fluo-4–based Ca^{2+} imaging experiments and whole-cell patch clamping. As expected, riluzole induced strong Ca^{2+} signals in MMECs from WT but not TRPC5$^{-/-}$ mice (Fig. 4*A*). This effect was independent of the filling state of the intracellular Ca^{2+} stores because these were depleted with thapsigargin before riluzole delivery. Whole-cell patch clamp measurements also confirmed the successful activation of TRPC5 channels by riluzole in MMECs (Fig. 4*B*).

To test whether riluzole can enhance EC sprouting, we assayed spheroid capillary sprouting and angiogenic sprouting in MMECs treated with riluzole compared with treatment with clemizole, a TRPC5 inhibitor (34). As expected, riluzole enhanced EC sprouting (Fig. 4, *C* and *D*), whereas the TRPC5 inhibitor clemizole abolished EC sprouting (Fig. 4, *C* and *D*). These results demonstrate that the approved drug riluzole is an effective TRPC5 activator that can promote EC sprouting *in vitro*.

To investigate whether riluzole can promote recovery from ischemia, we used the mouse HLI model. Laser Doppler imaging showed that restoration of blood perfusion in the hind limbs of mice treated with riluzole was improved compared with control mice (Fig. 4*E*). We also confirmed the specificity of riluzole's effect on activating TRPC5 in the mouse HLI model. Under treatment with riluzole, the restoration of hind limb blood perfusion of TRPC5$^{-/-}$ mice was still slower compared with WT mice (Fig. S4), which means that riluzole targets TRPC5 to show its effect in ischemic injury. Moreover, we found significantly higher blood vessel densities in the adductor muscles of riluzole-treated mice (Fig. 4*F*). These results demonstrated that activating TRPC5 with the approved drug riluzole promotes ischemic tissue recovery. In conclusion, we have demonstrated that TRPC5 plays a role in angiogenesis that may involve the NFATc3–ANGPT1 pathway and that the TRPC5 activator riluzole may be a therapeutic candidate to promote ischemic tissue recovery (Fig. 4*G*).

Discussion

Ca^{2+}-permeable ion channels such as TRPC have been reported to play a vital role in EC functions and angiogenesis by regulating Ca^{2+} entry. However, no reports exist on whether TRPC channels can regulate angiogenesis in response to ischemic injury. In this study, we investigated whether TRPC channels are involved in hypoxia-related EC function and in ischemic tissue recovery by regulating angiogenesis. Our findings provide evidence that TRPC5 is involved in hypoxia-induced EC action and angiogenesis.

Both *in vitro* and *in vivo* experiments in this study showed that TRPC5 is an important regulator of EC function and angiogenic growth. TRPC5 knockout delayed vascular recovery in ischemic mouse retinas, as evidenced by increased avascular and NVT areas. Moreover, TRPC5 contributed to ischemia-induced adaptive pathophysiological angiogenesis and restored blood flow, promoting ischemic tissue recovery in a hind limb ischemia model. The regulation of angiogenesis by TRPC5 may be related to the downstream event of NFATc3 translocation from the cytosol to the nucleus, resulting in enhanced ANGPT1 expression, which, in turn, may promote angiogenesis. Riluzole, an FDA-approved drug and activator of TRPC5, improved ischemic tissue recovery in our model of HLI. Together, these results demonstrate a key role of TRPC5 in EC sprouting and angiogenesis under ischemic conditions. Moreover, activating TRPC5 by riluzole treatment is a promising option for treating ischemic injury.

Effective treatment options for ischemia–hypoxia–related diseases are limited. Although targeting angiogenic factors, such as VEGF, is an attractive strategy, and VEGF has shown optimistic results in the laboratory, clinical trial results of angiogenic cytokines for ischemic disease therapy are controversial and inconclusive (5, 10, 14, 15, 35, 36). In one study, adVEGF121 was delivered intramuscularly to the lower legs of patients with peripheral arterial disease. However, the primary and secondary endpoints were similar among the groups (16). The long-term results of VEGF gene transfer have also been suboptimal, as no significant differences in the cause of death or number of treated leg amputations were seen (17).The identification of additional treatment strategies is therefore urgent and important. Here we showed that the TRPC5 activator riluzole has promising effects in promoting angiogenesis in ischemic tissues of HLI mice. Our study showed that riluzole, an FDA-approved oral drug that is commonly used to treat ALS, can activate TRPC5 and trigger TRPC5-mediated Ca^{2+} influx in ECs. Riluzole promoted EC sprouting *in vitro*, whereas the TRPC5 inhibitor clemizole suppressed EC sprouting. Furthermore, we used a mouse HLI model to show that riluzole can effectively promote ischemic tissue recovery, revealing its potential therapeutic value. Riluzole is well-tolerated for long periods (37), and its repurposing for ischemic disease treatment shows great promise given the abbreviated drug development time and cost for FDA-approved drugs.

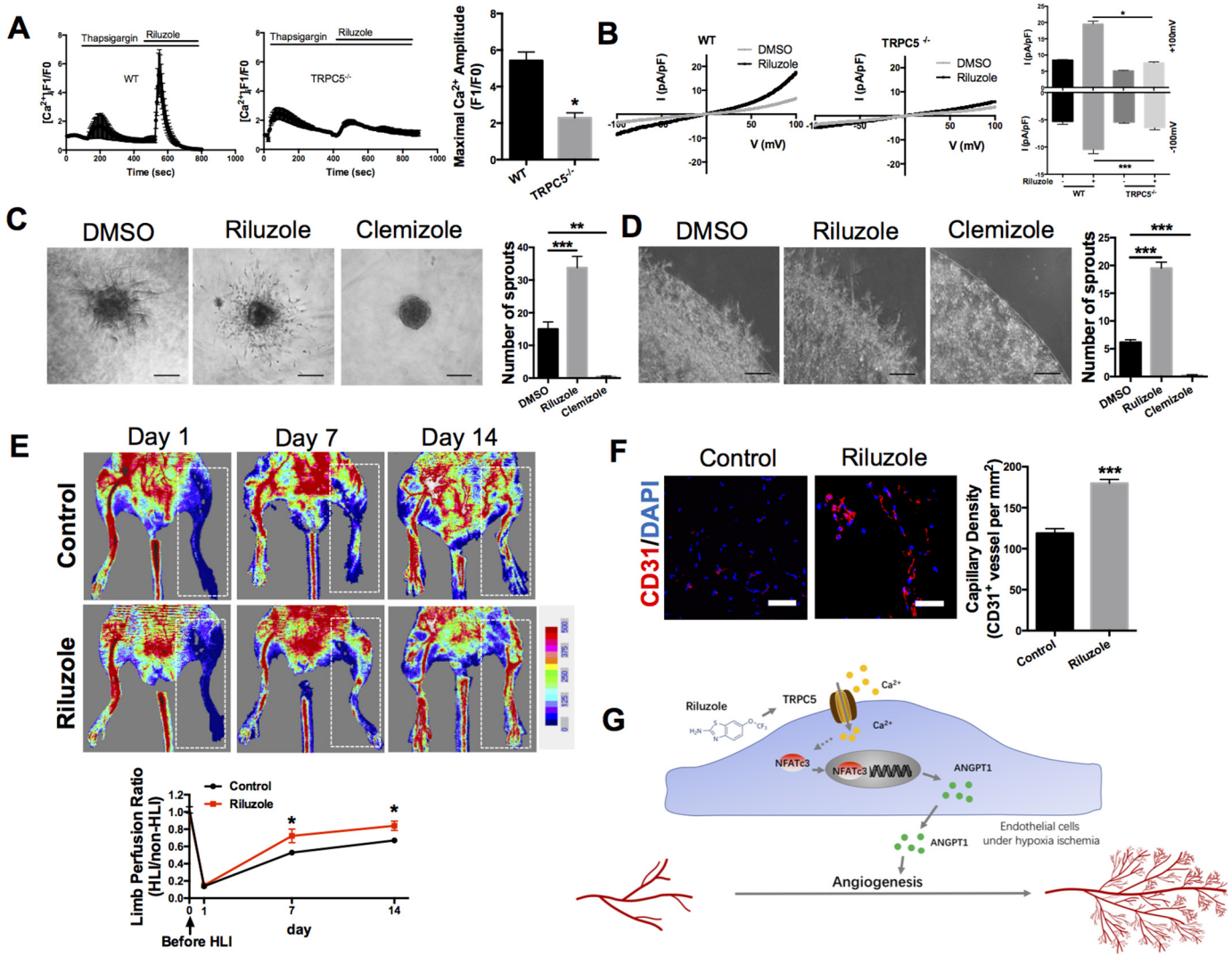

Figure 4. TRPC5 activation by riluzole promotes ischemic tissue recovery. *A*, representative measurement of $[Ca^{2+}]_i$ in Fluo-4-loaded MMECs from WT and TRPC5$^{-/-}$ mice. Internal Ca^{2+} stores were depleted with thapsigargin (2 μmol/liter) before riluzole (50 μmol/liter) was applied. The statistical analysis is shown on the *right*. The values are means ± S.E. of $n = 4$ independent experiments. *, $p < 0.05$ *versus* WT; unpaired Mann–Whitney test. For each experiment, 15–30 randomly chosen cells were analyzed. The maximum $[Ca^{2+}]_i$ response of each cell after riluzole treatment was detected. *B*, representative whole-cell recordings from WT and TRPC5$^{-/-}$ MMECs with the current–voltage curves for basal and riluzole-induced (50 μmol/liter) currents. The values are means ± S.E. of $n = 5$ independent experiments. *, $p < 0.05$; Kruskal–Wallis test and Dunn's multiple comparisons test. ***, $p < 0.001$, one-way ANOVA and Tukey's multiple comparisons test. *C* and *D*, *left panels*, representative images of sprouting spheroids (*C*, $n = 5$) or angiogenic sprouting assays (*D*, $n = 6$) in WT MMECs. For the angiogenic sprouting assay, duplex cultured cells in matrix membrane with riluzole (50 μmol/liter), clemizole (10 μmol/liter), or DMSO were incubated for 24 h. *Right panels*, morphometric analysis. **, $p < 0.01$; ***, $p < 0.001$; one-way ANOVA and Dunnett's multiple comparisons test. *E*, HLI was surgically induced. The restoration rates of hind limb blood flow after treatment with or without riluzole (10 mg/kg/day) were compared by laser Doppler imaging on day 7 and day 14 after ischemia. Ischemic limbs are highlighted by *white dashed boxes*. $n = 6$. *, $p < 0.05$ *versus* control on day 7; unpaired *t* test with Welch's correction. *, $p < 0.05$ *versus* control on day14, Student's unpaired two-tailed *t* test. *F*, immunofluorescence of CD31 (*left panel*) and summary data (*right panel*) in adductor muscle sections from the injured limbs on day 14 after HLI. $n = 6$. ***, $p < 0.001$ *versus* control; Student's unpaired two-tailed *t* test. *G*, schematic of the TRPC5–NFATc3–ANGPT1 signaling pathway in angiogenesis under ischemia. *A–F*, representative images are shown, means ± S.E. *Scale bars* = 100 μm (*C* and *D*) and 50 μm (*F*).

The underlying mechanisms behind TRPC5-mediated regulation in ischemia are likely to involve responses to hypoxia. It remains unknown whether TRPC5 is an oxygen-sensing channel that can respond to the low oxygen levels associated with ischemic injury. TRP channels have been studied as sensors and transducers of molecular O_2 signal (38). Recent studies have demonstrated that hypoxia and O_2 glucose deprivation can activate TRPC6 and TRPM7, respectively (38). TRPA1 can sense hyperoxia and mild hypoxia in vagal and sensory neurons (38). TRPC5 was also found to be activated by multiple other chemical factors (39). It has been demonstrated that NO and H_2O_2 can directly activate the TRPC5 channel by modification of cysteine residues, causing robust Ca^{2+} influx (40). Reduced thioredoxin activates TRPC5 by breaking its SS bond Cys^{553}-Cys^{558} in the putative extracellular loop near the pore region (39). In endothelial cells, TRPC5 is important for the Ca^{2+} influx activated by endothelial nitric oxide synthase (eNOS) produced NO via receptor–ATP stimulation (39). However, whether TRPC5 is oxygen-sensing and involved in acute or chronic hypoxia response of endothelial cells remains unknown. Additionally, it is possible that TRPC5 develops heteromers with other TRPCs to regulate angiogenesis under

ischemia. Assembly of TRPC homologs into heteromers can generate various channels (41). TRPC5 has been reported to assembled with TRPC1 and TRPC4 into heteromultimers in the mouse brain to regulate spatial working memory (42). Although TRPC5 may not form heteromultimers with TRPC6, the TRPC6–TRPC5 channel cascade has been found to regulate EC movement (43). Further studies are needed to test whether TRPC5 can form heteromultimers to regulate angiogenesis. Moreover, clinical studies are needed to validate the beneficial effect of riluzole in patients with ischemia-related diseases. As an FDA-approved drug, the new proposed use for riluzole in ischemia extends its clinical and translational value. Further studies are needed to identify the specific indications, safety, and efficacy for its use for conditions such as ischemic cardiovascular disease.

In conclusion, we present the first evidence that TRPC5 improves angiogenesis under hypoxia–ischemia. The FDA-approved drug riluzole promoted ischemic tissue recovery by activating TRPC5. These effects may be related to the TRPC5–NFATc3–ANGPT1 signaling pathway. Our study reveals TRPC5 as a new target and its activator riluzole as a promising drug for the clinical treatment of ischemia-related diseases.

Experimental procedures

Study design

The aims of our study were to investigate whether TRPC5 is involved in angiogenesis under ischemia–hypoxia conditions and to study the potential of the TRPC5 activator riluzole for treating ischemia-related diseases. For the first objective, we used TRPC5$^{-/-}$ and WT mice to analyze the effects of TRPC5 on EC sprouting and vascular recovery in ischemia models. For the second objective, we treated primary ECs and an HLI mouse model with riluzole and analyzed the effects on *in vitro* EC sprouting and *in vivo* ischemia tissue recovery. The underlying mechanisms were investigated with isolated primary ECs. The investigators who performed the genotyping were blind to the mouse genotypes. All experimental data from the TRPC5 transgenic mice were compared with those from the littermate controls. In the OIR experiments, the body weights of all mice were measured, and the outliers that were at least two standard deviations away from the mean body weight of their littermates were excluded to ensure that mice with similar body weights were compared.

Mice

TRPC5$^{-/-}$ and WT mice were a kind gift from Prof. David E. Clapham (Harvard Medical School, USA). Age- and sex-matched TRPC5$^{-/-}$ and WT littermates were selected by an established PCR genotyping method (Fig. S5) and used for this study (44). C57BL/6J mice were purchased from the Shanghai Laboratory Animal Center, Chinese Academy of Sciences (Shanghai, China). All mice were housed under air-filtered and pathogen-free conditions. All animal experiments were approved by the Animal Experimentation Ethics Committee of Jiangnan University and performed in compliance with the Guide for the Care and Use of Laboratory Animals (National Institutes of Health publication, 8th edition, updated 2011).

Cell cultures and transfection

Cells were obtained from the American Type Culture Collection. HEK293 cells were cultured in Dulbecco's modified Eagle's medium supplemented with 10% fetal bovine serum, 100 μg/ml penicillin, and 100 μg/ml streptomycin. HMECs and primary MMECs were cultured in endothelial cell growth medium (EGM) (Lonza, Basel, Switzerland). MMECs were isolated and cultured in EGM for 3–5 days. Primary MMECs without passage were used for the experiments.

Cells were transfected using Lipofectamine 2000 transfection reagent according to the manufacturer's instructions (Invitrogen). The siRNA sequences (GenePharma, Shanghai, China) were as follows (sense strand): siTRPC5-1, CCAAUGGACUGAACCAGCUUUACUU; siTRPC5-2, GGAGCUACCAUGUUUGGAATT; siNFATc3-1, CUGCCAUACUACCAGGAAATT; siNFATc3-2, CCGCAAUUCAGAUAUAGAATT; siNFATc3-3, CCGCAAUUCAGAUAUAGAATT; siTRPC1, CAGCCAGAUUCCUAGCUUU; siTRPC3, GGAAGAACUGCUCUCCUCAUUGCAA; siTRPC4, TCGAGGACCAGCATACATG; siTRPC6, TCGAGGACCAGCATACATG.

Spheroid capillary sprouting assay

Spheroid capillary sprouting assays were performed as described previously (45). Briefly, cells were suspended in EGM (CC-3162, Lonza) containing 0.25% (w/v) methylcellulose and seeded in nonadherent round-bottomed 96-well plates (3474, Corning, Kennebunk, ME). To establish hypoxic conditions, the cells were incubated with 1% O_2, 94% N_2, and 5% CO_2 at 37 °C in a humidified multigas incubator (4031, Thermo). Spheroids were allowed to form for 24 h under hypoxia and embedded into collagen gels to form sprouts under hypoxia. Sprout formation was examined 24 h after embedding with a video camera (Nikon Coolpix 54, Tokyo, Japan). The number of sprouts was determined for each spheroid. When indicated, the cells were transfected with siRNA for 48 h before seeding to form spheroids or treated with riluzole (50 μM) and clemizole (10 μM) during sprout formation.

Angiogenic sprouting assay

Angiogenic sprouting assays were performed as described in a previous report (46). Briefly, 5×10^5 mouse primary mesenteric endothelial cells were suspended in 25 μl of EGM and mixed at a 1:1 ratio with basement membrane matrix (354234, BD Biosciences). Next, 50-μl aliquots were spotted onto 4-well plates (Nunc, Roskilde, Denmark) and incubated at 37 °C for 30 min. When the basement membrane matrix had hardened, 2 ml of EGM was added to each well and incubated for 12 h. Then a second layer of Matrigel diluted 1:1 with EGM was superimposed on the primary spots to create duplex cultures; these samples were then incubated for 24 h. Riluzole (50 μM) or clemizole (10 μM) was added to the second layer of Matrigel. Images were captured with a video camera (Nikon Coolpix 54, Tokyo, Japan). The number of sprouts was determined for each spot.

$[Ca^{2+}]_i$ measurement

Endothelial cells were seeded on coverslips 12 h before measurement. The medium was removed, and the cells were

washed once with PBS. The cells were then incubated in the dark with 10 μM Fluo-4 (Invitrogen) and 0.02% Pluronic F-127 in normal physiological saline solution buffer at 37 °C for 30 min. The coverslips were rinsed with normal physiological saline solution and transferred to a bath chamber. In addition, the cells were pretreated with thapsigargin (2 μM) to deplete the inositol trisphosphate ($InsP_3$)–sensitive Ca^{2+} stores. Riluzole (50 μM) was used to activate TRPC5. Fluorescence intensity and signal relative to the starting signal (F1/F0 ratio) were measured using a confocal microscope (TCS SP8, Leica, Wetzlar, Germany).

Tube formation assay

Growth factor–reduced Matrigel was thawed at 4 °C overnight. Tips and 24-well plates were precooled at 4 °C for 2 h before the experiments. Twenty-four–well plates coated with 250 μl of Matrigel (354234, BD Biosciences) were incubated at 37 °C for 30 min until the Matrigel solidified. ECs (8×10^4) were then added to the plate and incubated at 37 °C for 6 h. To establish hypoxic conditions, the cells were incubated in 1% O_2, 94% N_2, and 5% CO_2 at 37 °C in a humidified multigas incubator (4031, Thermo). Tubular network images were captured with a video camera (Coolpix 54, Nikon, Tokyo, Japan) mounted on a microscope. Tube formation was quantified as the number of tubular structures in five randomly selected microscopic fields.

Hind limb ischemia model

Mice underwent unilateral femoral artery ligation (47). Briefly, following anesthesia with chloral hydrate (5%, 0.08 ml/10 g), the left femoral artery was exposed under a dissecting microscope. The proximal femoral artery and the distal portion of the saphenous artery were ligated, and an arteriectomy was performed. Blood flow was measured using a laser Doppler imaging system (Moor Instruments, Devon, UK). On day 14, the mice were sacrificed, and the adductor muscles were harvested to prepare frozen sections for immunofluorescence.

When indicated, an AAV carrying the gene of interest was injected at two sites in the adductor muscle and two sites in the gastrocnemius muscle 7 days before surgery (total AAV dose, 5×10^{10} pfu in 40 μl). Mice that received riluzole were administered the drug at 10 mg/kg/day intragastrically for 14 days after surgery.

OIR and postnatal analysis of retinal angiogenesis

The OIR mouse model was generated as indicated in a previous report (27). Briefly, mice on PD7 and their nursing mothers were exposed to 75% oxygen in a hyperoxic chamber (YCP-160D, Huaxi Electronic Technology, Changsha, China) for 5 days and then returned to room air for 5 days. Mouse retinal dissection and vascular analyses were performed according to a study by Pitulescu *et al.* (48). Briefly, the eyes were fixed in 4% paraformaldehyde (Sigma-Aldrich) and dissected under a microscope. After dissection, the retinas were stained with isolectin B4 (1:25) overnight at 4 °C. The samples were then analyzed under a Leica confocal microscope. Because the body weight of the pups is important for interpreting the retina phenotype and because growth retardation is reflected in vascular developmental delays, only pups with similar weights were used for the analyses.

Immunofluorescence analysis

Briefly, frozen sections were fixed in 4% paraformaldehyde (Sigma-Aldrich, St. Louis, MO) for 30 min. The samples were washed with PBS buffer and then blocked for 30 min with 5% BSA in PBS. The samples were incubated overnight with primary antibodies at 4 °C. A CD31 antibody (ab9498, Abcam, 1:50) was used for microvascular staining. Then the samples were incubated with secondary antibodies (ab175473, Abcam, 1:500) at room temperature for 2 h. 4′,6-Diamidino-2-phenylindole (1:1000 in PBS, 15 min at room temperature) was used for nuclear staining. Images were captured under a confocal microscope (Leica TCS SP8). For the microvessel density assessments, the vessel numbers were counted in five random fields in each of the four tissue sections (per mouse) and expressed as $CD31^+$ vessels per square millimeter.

Western blotting

Cells were lysed in radioimmune precipitation assay lysis buffer supplemented with fresh protease inhibitors (Roche). The protein concentrations were measured using a bicinchoninic acid protein assay kit (P0010, Beyotime, Shanghai, China). The proteins were then separated on an SDS-PAGE gel and transferred onto a polyvinylidene difluoride membrane. The membrane with transferred proteins was incubated overnight at 4 °C with primary antibodies (1:1000) in TBS with Tween 20 (TBST) buffer containing 5% fat-free milk. The following antibodies were used: anti-TRPC5 (ACC-020, Alomone), anti-angiopoietin 1 (ab183701, Abcam), anti-β-actin (ab8227, Abcam), and anti-NFATc3 (sc-8405, Santa Cruz Biotechnology). Then the membrane was incubated with a horseradish peroxidase–conjugated secondary antibody (1:1000) at room temperature for 2 h. Secondary fluorescently labeled antibodies were from Abcam. The blots were developed using an ECL substrate (P0018, Beyotime) and imaged using a Chemi-Doc XRS+ system (Bio-Rad).

Mouse angiogenesis antibody array and mouse angiopoietin-1 ELISA analysis

Serum samples from WT and $TRPC5^{-/-}$ mice were used for an angiogenesis antibody array analysis with a commercial kit (ARY015, R&D Systems, Minneapolis, MN) according to the manufacturer's instructions. Serum samples from mice 3 days after hind limb ischemia surgery or sham operation were used for angiopoietin-1 detection using a commercial ELISA kit (CSB-E07302m, Cusabio, Shanghai, China) according to the manufacturer's instructions.

Luciferase reporter assay

HEK293T cells were co-transfected with 0.2 μg of reporter plasmid (ANGPT1), 0.2 μg of expression plasmid (NFATc3), and 0.04 μg of pRL-CMV using Lipofectamine 2000 reagent (Invitrogen). After 48 h, the cells were harvested, and luciferase activity was measured with a Dual-Luciferase reporter assay system (Promega, Madison, WI) in which the *Renilla* luciferase activity of pRL-CMV served as a control.

Whole-cell patch clamp analysis

Whole-cell patch clamping was conducted using an EPC10 patch clamp amplifier (HEKA, Holliston, MA) as described previously (49). The pipette solution contained 130 mM cesium aspartate, 2 mM $MgCl_2$, 5 mM Na_2 ATP, 5.9 mM $CaCl_2$, 10 mM EGTA, and 10 mM HEPES (pH 7.2) with CsOH. The bath solution contained 65 mM sodium aspartate, 5 mM KCl, 1 mM $CaCl_2$, 1 mM $MgCl_2$, 10 mM HEPES, and 10 mM glucose (pH 7.4) with NaOH. The TRPC5 current–voltage relationships of primary mesenteric endothelial cells were obtained using a 500-ms ramp protocol from −100 mV to +100 mV from a holding potential of −60 mV. The cells were treated with 50 μM riluzole or DMSO as a control in the bath solution.

Quantitative real time-PCR analysis

Total RNA was extracted with TRIzol according to the manufacturer's instructions (Invitrogen). RNA was dissolved in diethylpyrocarbonate-treated water. Samples of 1 μg of DNase-treated RNA were reverse-transcribed using the PrimeScript RT Reagent Kit (Takara, RR047A). The sequences of primers used to amplify the cDNA are listed in Table S1. Quantitative PCR was performed using SYBR Green mixture (Takara, RR890A) with cycling conditions of 95 °C for 30 s, followed by 40 cycles of 95 °C for 5 s and 60 °C for 30 s by real-time PCR cycler (Light Cycler 480 II, Roche).

Statistical analyses

All data are presented as the means ± S.E. Statistical analyses were performed using GraphPad Prism 6.0 software. For data passing normality and equal variance tests, comparisons between two groups were measured by Student's unpaired two-tailed *t* test, and differences among three or more groups were examined by one-way analysis of variance (ANOVA) followed by Dunnett's multiple comparisons test or Tukey's multiple comparisons test. Appropriate nonparametric tests were performed when either test failed. $p < 0.05$ was considered significantly different.

Author contributions—Y. Z., T. Z., and X. M. conceptualization; Y. Z., M. G., M. X., and A. M. data curation; Y. Z., M. G., M. X., and A. M. software; Y. Z., M. G., M. X., and A. M. formal analysis; Y. Z., X. Y., W. T. W., and X. M. supervision; Y. Z. validation; Y. Z., M. G., T. Z., M. X., and A. M. investigation; Y. Z., M. G., T. Z., M. X., and A. M. visualization; Y. Z., M. G., M. X., A. M., and L. F. methodology; Y. Z. and M. X. writing-original draft; Y. Z., T. Z., and X. M. project administration; Y. Z., X. Y., W. T. W., and X. M. writing-review and editing; X. M. resources; X. M. funding acquisition.

Acknowledgments—We thank Prof. David E. Clapham (Harvard Medical School) for sharing the TRPC5 transgenic mice and Prof. Iain C. Bruce (University of Hong Kong) for support with manuscript writing.

References

1. Roth, G. A., Johnson, C., Abajobir, A., Abd-Allah, F., Abera, S. F., Abyu, G., Ahmed, M., Aksut, B., Alam, T., Alam, K., Alla, F., Alvis-Guzman, N., Amrock, S., Ansari, H., Arnlov, J., *et al.* (2017) Global, regional, and national burden of cardiovascular diseases for 10 causes, 1990 to 2015. *J. Am. Coll. Cardiol.* **70,** 1–25 CrossRef Medline
2. GBD 2015 Mortality and Causes of Death Collaborators (2016) Global, regional, and national life expectancy, all-cause mortality, and cause-specific mortality for 249 causes of death, 1980–2015: a systematic analysis for the Global Burden of Disease Study 2015. *Lancet* **388,** 1459–1544 CrossRef Medline
3. Armstrong, E. J., Chen, D. C., Westin, G. G., Singh, S., McCoach, C. E., Bang, H., Yeo, K. K., Anderson, D., Amsterdam, E. A., and Laird, J. R. (2014) Adherence to guideline-recommended therapy is associated with decreased major adverse cardiovascular events and major adverse limb events among patients with peripheral arterial disease. *J. Am. Heart Assoc.* **3,** e000697 Medline
4. Albrecht-Schgoer, K., Barthelmes, J., Schgoer, W., Theurl, M., Nardin, I., Lener, D., Gutmann, C., Dünnhaupt, S., Bernkop-Schnürch, A., and Kirchmair, R. (2017) Nanoparticular delivery system for a secretoneurin derivative induces angiogenesis in a hind limb ischemia model. *J. Control. Release* **250,** 1–8 CrossRef Medline
5. Suzuki, J., Shimamura, M., Suda, H., Wakayama, K., Kumagai, H., Ikeda, Y., Akazawa, H., Isobe, M., Komuro, I., and Morishita, R. (2016) Current therapies and investigational drugs for peripheral arterial disease. *Hypertens. Res.* **39,** 183–191 CrossRef Medline
6. Wiviott, S. D., and Antman, E. M. (2004) Clopidogrel resistance. *Circulation* **109,** 3064 CrossRef Medline
7. Velazquez, E. J., Lee, K. L., Jones, R. H., Al-Khalidi, H. R., Hill, J. A., Panza, J. A., Michler, R. E., Bonow, R. O., Doenst, T., Petrie, M. C., Oh, J. K., She, L., Moore, V. L., Desvigne-Nickens, P., Sopko, G., *et al.* (2016) Coronary-artery bypass surgery in patients with ischemic cardiomyopathy. *N. Engl. J. Med.* **374,** 1511–1520 CrossRef Medline
8. Menard, M. T., Farber, A., Assmann, S. F., Choudhry, N. K., Conte, M. S., Creager, M. A., Dake, M. D., Jaff, M. R., Kaufman, J. A., Powell, R. J., Reid, D. M., Siami, F. S., Sopko, G., White, C. J., and Rosenfield, K. (2016) Design and rationale of the best endovascular versus best surgical therapy for patients with critical limb ischemia (BEST-CLI) Trial. *J. Am. Heart Assoc.* **5,** e003219 CrossRef Medline
9. Vartanian, S. M., and Conte, M. S. (2015) Surgical intervention for peripheral arterial disease. *Circ. Res.* **116,** 1614–1628 CrossRef Medline
10. Ylä-Herttuala, S., Bridges, C., Katz, M. G., and Korpisalo, P. (2017) Angiogenic gene therapy in cardiovascular diseases: dream or vision? *Eur. Heart J.* **38,** 1365–1371 Medline
11. Saharinen, P., Eklund, L., and Alitalo, K. (2017) Therapeutic targeting of the angiopoietin-TIE pathway. *Nat. Rev. Drug Discov.* **16,** 635–661 CrossRef Medline
12. Makarevich, P. I., and Parfyonova, Y. V. (2017) in *Physiologic and Pathologic Angiogenesis* (Simionescu, D. S., ed.), pp. 344–364, IntechOpen, London
13. Briquez, P. S., Clegg, L. E., Martino, M. M., Gabhann, F. M., and Hubbell, J. A. (2016) Design principles for therapeutic angiogenic materials. *Nat. Rev. Materials* **1,** 15006 CrossRef
14. Khurana, R., Simons, M., Martin, J. F., and Zachary, I. C. (2005) Role of angiogenesis in cardiovascular disease: a critical appraisal. *Circulation* **112,** 1813–1824 CrossRef Medline
15. Mathiyalagan, P., Liang, Y., Kim, D., Misener, S., Thorne, T., Kamide, C. E., Klyachko, E., Losordo, D. W., Hajjar, R. J., and Sahoo, S. (2017) Angiogenic mechanisms of human $CD34^+$ Stem cell exosomes in the repair of ischemic hindlimb. *Circ. Res.* **120,** 1466–1476 CrossRef Medline
16. Rajagopalan, S., Mohler, E. R., 3rd, Lederman, R. J., Mendelsohn, F. O., Saucedo, J. F., Goldman, C. K., Blebea, J., Macko, J., Kessler, P. D., Rasmussen, H. S., and Annex, B. H. (2003) Regional angiogenesis with vascular endothelial growth factor in peripheral arterial disease: a phase II randomized, double-blind, controlled study of adenoviral delivery of vascular endothelial growth factor 121 in patients with disabling intermittent claudication. *Circulation* **108,** 1933–1938 CrossRef Medline
17. Muona, K., Mäkinen, K., Hedman, M., Manninen, H., and Ylä-Herttuala, S. (2012) 10-year safety follow-up in patients with local VEGF gene transfer to ischemic lower limb. *Gene Ther.* **19,** 392–395 CrossRef Medline
18. Li, J., Cubbon, R. M., Wilson, L. A., Amer, M. S., McKeown, L., Hou, B., Majeed, Y., Tumova, S., Seymour, V. A., Taylor, H., Stacey, M., O'Regan, D., Foster, R., Porter, K. E., Kearney, M. T., and Beech, D. J. (2011) Orai1

and CRAC channel dependence of VEGF-activated Ca^{2+} entry and endothelial tube formation. *Circ. Res.* **108,** 1190–1198 CrossRef Medline
19. Noren, D. P., Chou, W. H., Lee, S. H., Qutub, A. A., Warmflash, A., Wagner, D. S., Popel, A. S., and Levchenko, A. (2016) Endothelial cells decode VEGF-mediated Ca^{2+} signaling patterns to produce distinct functional responses. *Sci. Signal.* **9,** ra20 CrossRef Medline
20. Gaunt, H. J., Vasudev, N. S., and Beech, D. J. (2016) Transient receptor potential canonical 4 and 5 proteins as targets in cancer therapeutics. *Eur. Biophys. J.* **45,** 611–620 CrossRef Medline
21. Li, J., Bruns, A. F., Hou, B., Rode, B., Webster, P. J., Bailey, M. A., Appleby, H. L., Moss, N. K., Ritchie, J. E., Yuldasheva, N. Y., Tumova, S., Quinney, M., McKeown, L., Taylor, H., Prasad, K. R., *et al.* (2015) Orai3 surface accumulation and calcium entry evoked by vascular endothelial growth factor. *Arterioscler. Thromb. Vasc. Biol.* **35,** 1987–1994 CrossRef Medline
22. Bruns, A., Li, J., Hou, B., Turnover, S., Moss, N., Mckeown, L., Foster, R., and Beech, D. (2014) Vascular endothelial growth factor A evokes distinct calcium entry by promoting surface accumulation of Orai3 (1057.5). *FASEB J.* **28,** 1057.1055
23. Antigny, F., Girardin, N., and Frieden, M. (2012) Transient receptor potential canonical channels are required for *in vitro* endothelial tube formation. *J. Biol. Chem.* **287,** 5917–5927 CrossRef Medline
24. Yu, P. C., Gu, S. Y., Bu, J. W., and Du, J. L. (2010) TRPC1 is essential for *in vivo* angiogenesis in zebrafish. *Circ. Res.* **106,** 1221–1232 CrossRef Medline
25. Veliceasa, D., Ivanovic, M., Hoepfner, F. T., Thumbikat, P., Volpert, O. V., and Smith, N. D. (2007) Transient potential receptor channel 4 controls thrombospondin-1 secretion and angiogenesis in renal cell carcinoma. *FEBS J.* **274,** 6365–6377 CrossRef Medline
26. Ge, R., Tai, Y., Sun, Y., Zhou, K., Yang, S., Cheng, T., Zou, Q., Shen, F., and Wang, Y. (2009) Critical role of TRPC6 channels in VEGF-mediated angiogenesis. *Cancer Lett* **283,** 43–51 CrossRef Medline
27. Lee, J., Kim, K. E., Choi, D. K., Jang, J. Y., Jung, J. J., Kiyonari, H., Shioi, G., Chang, W., Suda, T., Mochizuki, N., Nakaoka, Y., Komuro, I., Yoo, O. J., and Koh, G. Y. (2013) Angiopoietin-1 guides directional angiogenesis through integrin $\alpha v\beta 5$ signaling for recovery of ischemic retinopathy. *Sci. Transl. Med.* **5,** 203ra127 Medline
28. Stahl, A., Connor, K. M., Sapieha, P., Chen, J., Dennison, R. J., Krah, N. M., Seaward, M. R., Willett, K. L., Aderman, C. M., Guerin, K. I., Hua, J., Löfqvist, C., Hellström, A., and Smith, L. E. (2010) The mouse retina as an angiogenesis model. *Invest. Ophthalmol. Vis. Sci.* **51,** 2813–2826 CrossRef Medline
29. Dal Monte, M., Cammalleri, M., Mattei, E., Filippi, L., and Bagnoli, P. (2014) Protective effects of $\beta 1/2$ adrenergic receptor deletion in a model of oxygen-induced retinopathy. *Invest. Ophthalmol. Vis. Sci.* **56,** 59–73 Medline
30. Metheny-Barlow, L. J., and Li, L. Y. (2003) The enigmatic role of angiopoietin-1 in tumor angiogenesis. *Cell Res.* **13,** 309–317 CrossRef Medline
31. Ma, X., Cai, Y., He, D., Zou, C., Zhang, P., Lo, C. Y., Xu, Z., Chan, F. L., Yu, S., Chen, Y., Zhu, R., Lei, J., Jin, J., and Yao, X. (2012) Transient receptor potential channel TRPC5 is essential for P-glycoprotein induction in drug-resistant cancer cells. *Proc. Natl. Acad. Sci. U.S.A.* **109,** 16282–16287 CrossRef Medline
32. Richter, J. M., Schaefer, M., and Hill, K. (2014) Riluzole activates TRPC5 channels independently of PLC activity. *Br. J. Pharmacol.* **171,** 158–170 CrossRef Medline
33. Naylor, J., Minard, A., Gaunt, H. J., Amer, M. S., Wilson, L. A., Migliore, M., Cheung, S. Y., Rubaiy, H. N., Blythe, N. M., Musialowski, K. E., Ludlow, M. J., Evans, W. D., Green, B. L., Yang, H., You, Y., *et al.* (2016) Natural and synthetic flavonoid modulation of TRPC5 channels. *Br. J. Pharmacol.* **173,** 562–574 CrossRef Medline
34. Richter, J. M., Schaefer, M., and Hill, K. (2014) Clemizole hydrochloride is a novel and potent inhibitor of transient receptor potential channel TRPC5. *Mol. Pharmacol.* **86,** 514–521 CrossRef Medline
35. Zhang, Z. G., and Chopp, M. (2009) Neurorestorative therapies for stroke: underlying mechanisms and translation to the clinic. *Lancet Neurol.* **8,** 491–500 CrossRef Medline
36. Kusumanto, Y. H., van Weel, V., Mulder, N. H., Smit, A. J., van den Dungen, J. J., Hooymans, J. M., Sluiter, W. J., Tio, R. A., Quax, P. H., Gans, R. O., Dullaart, R. P., and Hospers, G. A. (2006) Treatment with intramuscular vascular endothelial growth factor gene compared with placebo for patients with diabetes mellitus and critical limb ischemia: a double-blind randomized trial. *Human Gene Ther.* **17,** 683–691 CrossRef Medline
37. Lacomblez, L., Bensimon, G., Leigh, P. N., Debove, C., Bejuit, R., Truffinet, P., Meininger, V., and ALS Study Groups I and II (2002) Long-term safety of riluzole in amyotrophic lateral sclerosis. *Amyotroph. Lateral Scler. Other Motor Neuron Disord.* **3,** 23–29 CrossRef Medline
38. Takahashi, N., Kozai, D., and Mori, Y. (2012) TRP channels: sensors and transducers of gasotransmitter signals. *Front. Physiol.* **3,** 324 Medline
39. Nilius, B., and Flockerzi, V. (2014) Mammalian transient receptor potential (TRP) cation channels. Preface. *Handb. Exp. Pharmacol.* **223,** v–vi Medline
40. Ogawa, N., Kurokawa, T., and Mori, Y. (2016) Sensing of redox status by TRP channels. *Cell Calcium* **60,** 115–122 CrossRef Medline
41. Strübing, C., Krapivinsky, G., Krapivinsky, L., and Clapham, D. E. (2003) Formation of novel TRPC channels by complex subunit interactions in embryonic brain. *J. Biol. Chem.* **278,** 39014–39019 CrossRef Medline
42. Broker-Lai, J., Kollewe, A., Schindeldecker, B., Pohle, J., Nguyen Chi, V., Mathar, I., Guzman, R., Schwarz, Y., Lai, A., Weissgerber, P., Schwegler, H., Dietrich, A., Both, M., Sprengel, R., Draguhn, A., *et al.* (2017) Heteromeric channels formed by TRPC1, TRPC4 and TRPC5 define hippocampal synaptic transmission and working memory. *EMBO J.* **36,** 2770–2789 CrossRef Medline
43. Chaudhuri, P., Colles, S. M., Bhat, M., Van Wagoner, D. R., Birnbaumer, L., and Graham, L. M. (2008) Elucidation of a TRPC6-TRPC5 channel cascade that restricts endothelial cell movement. *Mol. Biol. Cell* **19,** 3203–3211 CrossRef Medline
44. Riccio, A., Li, Y., Moon, J., Kim, K. S., Smith, K. S., Rudolph, U., Gapon, S., Yao, G. L., Tsvetkov, E., Rodig, S. J., Van't Veer, A., Meloni, E. G., Carlezon, W. A., Jr., Bolshakov, V. Y., and Clapham, D. E. (2009) Essential role for TRPC5 in amygdala function and fear-related behavior. *Cell* **137,** 761–772 CrossRef Medline
45. Korff, T., Krauss, T., and Augustin, H. G. (2004) Three-dimensional spheroidal culture of cytotrophoblast cells mimics the phenotype and differentiation of cytotrophoblasts from normal and preeclamptic pregnancies. *Exp. Cell Res.* **297,** 415–423 CrossRef Medline
46. Banumathi, E., O'Connor, A., Gurunathan, S., Simpson, D. A., McGeown, J. G., and Curtis, T. M. (2011) VEGF-induced retinal angiogenic signaling is critically dependent on Ca^{2+} signaling by Ca^{2+}/calmodulin-dependent protein kinase II. *Invest. Ophthalmol. Vis. Sci.* **52,** 3103–3111 CrossRef Medline
47. Niiyama, H., Huang, N. F., Rollins, M. D., and Cooke, J. P. (2009) Murine model of hindlimb ischemia. *J. Vis. Exp.* 1035
48. Pitulescu, M. E., Schmidt, I., Benedito, R., and Adams, R. H. (2010) Inducible gene targeting in the neonatal vasculature and analysis of retinal angiogenesis in mice. *Nat. Protoc.* **5,** 1518–1534 CrossRef Medline
49. Wong, C. O., Sukumar, P., Beech, D. J., and Yao, X. (2010) Nitric oxide lacks direct effect on TRPC5 channels but suppresses endogenous TRPC5-containing channels in endothelial cells. *Pflugers Arch.* **460,** 121–130 CrossRef Medline